Evaluating New and Current Horizontal Protection Levels in the Baseline ARAIM Algorithm

Danielle Racelis, Mathieu Joerger *Virginia Tech*

BIOGRAPHY

Danielle Racelis (B.S., University of the Philippines, 2014; B.S., M.S., University of Arizona, 2017, 2019) is a PhD candidate at Virginia Tech, working with Dr. Mathieu Joerger on navigation integrity using multi-constellation GNSS and LEO satellite constellations, in the Navigation laboratory for Autonomous Vehicle inTegrity (NAViTi).

Dr. Mathieu Joerger (M.S., INSA Strasbourg - Illinois Tech, 2002; Ph.D., Illinois Tech 2009) is assistant professor at Virginia Tech, senior editor of Navigation for IEEE TAES, and a member of the EU/US Cooperation on Satellite Navigation, Working Group C - ARAIM.

ABSTRACT

The baseline algorithm for horizontal advanced receiver autonomous integrity monitoring (HARAIM) provides one acceptable means of computing a horizontal protection level (HPL) that meets the safety requirements for aircraft en-route navigation. The baseline HARAIM algorithm iteratively solves for a single protection level across all hypotheses, which is equivalent to optimally allocating the integrity risk requirement across all hypotheses for PL evaluation. This optimization process is separately carried out twice, in the East and North directions. In this paper, we perform this iterative process only once: we show that it is computationally more efficient and can provide a tighter bound on horizontal radial positioning errors than the baseline HPL. We derive a generalized chi-square formulation of the HPL to quantify the tightness of both the baseline and the proposed HPL bounds. We conduct a worldwide risk analysis to compare baseline, and new HPL approaches in terms of coverage of 100% availability.

I. INTRODUCTION

The advanced receiver autonomous integrity monitoring (ARAIM) baseline algorithm provides probabilistic positioning error bounds which account for the impact of both nominal errors and undetected faults (Working Group C (WGC), 2016).

These positioning error bounds come in the form of a horizontal protection level (HPL) for Horizonatal ARAIM (HARAIM) and Vertical ARAIM (VARAIM) and a vertical protection level (VPL) for VARAIM. Together, HPL and VPL describe a cylinder centered at the true user location and containing the estimated location with a very high confidence, for example 99.99999% (Working Group C (WGC), 2022). The baseline algorithm was developed over the last decade with an initial focus on VARAIM for vertical guidance of aircraft during approach (Working Group C (WGC), 2016) that shifted towards HARAIM for aircraft en route navigation (Working Group C (WGC), 2022). This paper addresses the HARAIM HPL. The current ARAIM Algorithm Description Document (ADD) provides one acceptable means of computing an HPL that meets safety requirements (Working Group C (WGC), 2022). While alternative HPL equations exist (Walter and Enge, 1995; Ober, 1997; Jiang and Wang, 2016), they are not as tightly bounding, nor as computationally efficient as the ARAIM baseline algorithm.

According to the Satellite Based Augmentation Systems (SBAS) Minimum Operational Performance Standards (MOPS) for GPS, the HPL is defined as the horizontal radius of a circle, centered at the true position, which is expected to contain the estimated horizontal position at a probability defined by the integrity and continuity requirements (Radio Technical Commission for Aeronautics (RTCA) Special Committee 159, 2009). We denote the two-dimensional horizontal positioning error (HPE) vector as $\boldsymbol{\varepsilon}$, and define the HPL as

$$P\left(\|\boldsymbol{\varepsilon}\| \geq HPL\right) = P_{Alloc} \tag{1}$$

where the parameter HPL is the radius of a circle such that the probability of the radial error, $\|\boldsymbol{\varepsilon}\| = \sqrt{\boldsymbol{\varepsilon}^{\mathrm{T}}\boldsymbol{\varepsilon}}$, exceeding HPL is equal to a predefined risk requirement allocation, P_{Alloc}. This risk allocation is application-dependent, and is on the order of 10^{-7} for HARAIM.

The SBAS MOPS justifies deriving *HPL* from a 1D normal distribution along the worst-case horizontal direction. In contrast, the baseline ARAIM algorithm evaluates two protection levels for two 1D normal distributions aligned to the East and North directions respectively, and then combines the two PLs to conservatively produce an HPL (Working Group C (WGC), 2022; Blanch et al., 2015).

In this paper, we point out one step in the baseline HPL computation that can be modified to increase the tightness of the bound while reducing computation load. We first evaluate the tightness of the baseline HPL by comparing it to a tighter, generalized chi-square HPL formulation. Then, we derive a new, more computationally-efficient, and tighter HPL. Finally, we quantify ARAIM availability performance for both the baseline and the new HPL approaches.

II. HPL AND HPE FUNDAMENTALS

1. Baseline HPL Bound

The distribution of horizontal positioning error (HPE) samples is represented in Fig. 1. The baseline ARAIM algorithm computes East and North protection levels considering two 1D normal distributions, where each direction is allotted half the risk allocation. This approach can be expressed as:

$$P\left(|\varepsilon_E| \geq PL_E\right) = \frac{1}{2} P_{Alloc} \tag{2}$$

$$P\left(|\varepsilon_N| \geq PL_N\right) = \frac{1}{2} P_{Alloc} \ . \tag{3}$$

The left-hand-side probabilities in Eq. 2 and 3 are represented by two pairs of half planes in Fig. 1. The risk of being in one *or* the other half-plane-pair is smaller than P_{Alloc} because the risks of being in any one of the four dark-gray quadrants is double-counted.

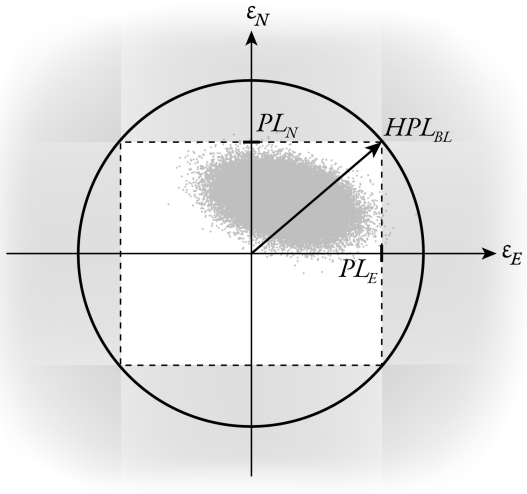

Figure 1: Example horizontal positioning error sample distribution and baseline horizontal protection level

The baseline HPL is defined as: $HPL_{BL} = \sqrt{PL_E^2 + PL_N^2}$ (Working Group C (WGC), 2016). Figure 1 shows that HPL_{BL} is bounding: if the probability of being outside the dashed rectangle is smaller than P_{Alloc}, then the risk of being outside the circle is even smaller. In mathematical terms, the probability of the radial HPE ($\sqrt{\varepsilon_E^2 + \varepsilon_N^2}$) exceeding HPL_{BL} can be bounded by the following expression:

$$P\left(\sqrt{\varepsilon_E^2 + \varepsilon_N^2} \geq HPL_{BL}\right) < P\left(|\varepsilon_E| \geq PL_E\right) + P\left(|\varepsilon_N| \geq PL_N\right) \ . \tag{4}$$

A tighter bound is possible as evidenced by the overlapping areas and by the regions that fall inside the HPL_{BL} circle.

2. Horizontal Positioning Error Model

We model the two-dimensional horizontal positioning error (HPE) as:

$$\boldsymbol{\varepsilon} = \boldsymbol{\varepsilon}_a + \boldsymbol{\varepsilon}_e \ . \tag{5}$$

where $\boldsymbol{\varepsilon}_a$ and $\boldsymbol{\varepsilon}_e$ respectively are the aleatory and epsitemic error components. $\boldsymbol{\varepsilon}_a$, captures uncertainty due to probabilistic variations, including those caused by measurement errors and modeled using Gaussian overbounds. This error component is modeled as

$$\boldsymbol{\varepsilon}_a \sim N\left(\mathbf{0}, \mathbf{P} = \begin{bmatrix} \sigma_E^2 & \sigma_{EN} \\ \sigma_{EN} & \sigma_N^2 \end{bmatrix}\right) \ . \tag{6}$$

$\boldsymbol{\varepsilon}_e$, captures uncertainty due to lack of knowledge. It is used in ARAIM to account for undetected faults and nominal errors due to signal deformation. This component can be bounded by the interval

$$-\mathbf{d} \leq \boldsymbol{\varepsilon}_e \leq \mathbf{d} \tag{7}$$

where $\mathbf{d} = \begin{bmatrix} d_E & d_N \end{bmatrix}^{\mathrm{T}}$. Equation (7) is an element-wise inequality, where the East and North epistemic error components are bounded by d_E and d_N respectively. Taking the magnitude of both sides of Eq. (5), we can leverage the triangle inequality to bound the radial error, as follows

$$\|\boldsymbol{\varepsilon}\| \leq \|\boldsymbol{\varepsilon}_a\| + \|\boldsymbol{\varepsilon}_e\| \tag{8}$$

where $\|\boldsymbol{\varepsilon}_e\|^2 = d_E^2 + d_N^2$. We choose to split the HPE into these two error components to aid in our derivation.

III. EVALUATING TIGHTNESS OF THE BASELINE HPL

1. Baseline HPL Notation

The baseline ARAIM algorithm assumes Gaussian overbounds in Eq. (2)-(3) and computes HPL using the following equations:

$$PL_E = k\sigma_E + d_E \tag{9}$$

$$PL_N = k\sigma_N + d_N \tag{10}$$

$$HPL_{BL}^2 = PL_E^2 + {PL_N}^2 \tag{11}$$

where k is the inverse of the tail probability of a standard normal distribution at a quarter of the risk allocation, that is $k = Q^{-1}\left(\frac{1}{4}P_{Alloc}\right)$. The first P_{Alloc}-halving is due to equal risk allocation between East and North directions. The second halving is to account for both tails of the normal distribution. (The baseline ARAIM algorithm has several refinements that are not directly significant to this derivation (Working Group C (WGC), 2022).) Expanding Eq. (11) and rearranging terms, HPL_{BL} can be written as:

$$HPL_{BL}^2 = k^2\left(\sigma_E^2 + \sigma_N^2\right) + \left\{2k\left(\sigma_E d_E + \sigma_N d_N\right) + d_E^2 + d_N^2\right\} \ . \tag{12}$$

The term in the squiggly brackets is an upper bound on $\|\boldsymbol{\varepsilon}_e\|^2$. The remainder of Section III evaluates the tightness of HPL_{BL} considering its aleatory component defined as:

$$HPL_{BL,a}^2 = k^2\left(\sigma_E^2 + \sigma_N^2\right) \tag{13}$$

2. Generalized Chi-Square-Based HPL

This section aims at showing that the squared radial HPE $\|\boldsymbol{\varepsilon}_a\|^2$ follows a *generalized* chi-square distribution. While it may be tempting to scale the East and North axes to obtain a chi-square distributed radial error distribution, the resulting HPL would become an ellipse instead of a circle, which would not comply with the HPL definition (Radio Technical Commission for Aeronautics (RTCA) Special Committee 159, 2009).

First, the eigen-decomposition of the covariance matrix $\mathbf{P}$ of the bivariate normal vector $\boldsymbol{\varepsilon}_a$ in Eq. (6) is given by:

$$\mathbf{P} = \mathbf{U}\boldsymbol{\Lambda}\mathbf{U}^{\mathrm{T}} \tag{14}$$

where $\mathbf{U}$ is an orthonormal matrix composed of the eigenvectors of the symmetric positive definite matrix $\mathbf{P}$ (i.e., $\mathbf{U}^{-1} = \mathbf{U}^{\mathrm{T}}$, $\mathbf{U}^{\mathrm{T}}\mathbf{U} = \mathbf{I}$), and $\boldsymbol{\Lambda}$ is a diagonal matrix with diagonal elements the eigenvalues of $\mathbf{P}$: λ_1^2, and λ_2^2. We define vector $\mathbf{v}$ as:

$$\mathbf{v} = \begin{bmatrix} v_1 \\ v_2 \end{bmatrix} = \mathbf{U}^{\mathrm{T}}\mathbf{P}^{-\frac{1}{2}}\boldsymbol{\varepsilon}_a \sim N\left(\mathbf{0}, \mathbf{I}\right) \tag{15}$$

where $\mathbf{P}^{-\frac{1}{2}}$ is the inverse of the principal square root of the covariance matrix. We obtain the following expression:

$$\|\boldsymbol{\varepsilon}_a\|^2 = \mathbf{v}^{\mathrm{T}}\boldsymbol{\Lambda}\mathbf{v} = \lambda_1^2 v_1^2 + \lambda_2^2 v_2^2 \tag{16}$$

where we have leveraged the fact that $\boldsymbol{\varepsilon}_a = \mathbf{P}^{\frac{1}{2}}\mathbf{U}\mathbf{v}$, and $\boldsymbol{\Lambda} = \mathbf{U}^{\mathrm{T}}\mathbf{P}\mathbf{U}$. Equation (16) is the expression of a generalized chi-square distribution, which is a weighted sum of squares of independent normal variables. The HPL equation for the aleatory HPE component becomes:

$$P\left(\|\boldsymbol{\varepsilon}_a\|^2 \geq HPL^2_{\widetilde{\chi^2},a}\right) = P_{Alloc} \tag{17}$$

where we use the entire risk allocation instead of halving it. This probability can be evaluated using numerical methods (Davies, 1980; Langel, 2021). $HPL_{\widetilde{\chi^2},a}$ provides a point of comparison to evaluate the tightness of $HPL_{BL,a}$.

The same numerical methods are applied in Sec. V, where we account for both aleatory and epistemic HPE components, by using Eq. (5) to form the complete $HPL^2_{\widetilde{\chi^2}}$. In Sec. V, the generalized chi-square distribution is a weighted sum of independent, non-zero mean, squared Gaussian variables.

3. Tightness of Baseline HPL for Any Satellite Geometry

We analyze tightness of the baseline HPL for different HPE covariance ellipses (satellite geometries), and different risk requirements. A measure of $HPL_{BL,a}$-tightness is given by the following ratio:

$$\frac{HPL_{BL,a}}{HPL_{\widetilde{\chi^2},a}} \tag{18}$$

which was shown in Fig.1 to be greater than 1, and approaches 1 when $HPL_{BL,a}$ is a tight HPE bound. In this section, we evaluate Eq. (18) with respect to two parameters that characterize the range of HPE covariance ellipse geometries: eccentricity, e ($e = \sqrt{1 - \frac{\lambda_2}{\lambda_1}}$, where $\lambda_2 < \lambda_1$), and orientation, θ (θ is the angle between the ellipse semimajor axis and the East axis). We can write the parametrized form of the covariance matrix as:

$$\mathbf{P} = \mathbf{U}\boldsymbol{\Lambda}\mathbf{U}^{\mathrm{T}} = \begin{bmatrix} -\sin\theta & \cos\theta \\ \cos\theta & \sin\theta \end{bmatrix} \begin{bmatrix} \lambda_1^2 & 0 \\ 0 & \lambda_2^2 \end{bmatrix} \begin{bmatrix} -\sin\theta & \cos\theta \\ \cos\theta & \sin\theta \end{bmatrix}^{\mathrm{T}} \tag{19}$$

$$= \begin{bmatrix} \lambda_1^2 \sin^2\theta + \lambda_2^2 \cos^2\theta & \left(\lambda_2^2 - \lambda_1^2\right)\sin\theta\cos\theta \\ \left(\lambda_2^2 - \lambda_1^2\right)\sin\theta\cos\theta & \lambda_1^2 \cos^2\theta + \lambda_2^2 \sin^2\theta \end{bmatrix}. \tag{20}$$

The HPL ratio in Eq. (18) is evaluated for a set of eccentricity and orientation values, $e \in [0, 1)$, and $\theta \in [0, 90°]$ respectively. We compute $HPL_{BL,a}$ from Eq. (13), and numerically solve for $HPL_{\widetilde{\chi^2},a}$ using Eq. (17) to get the results shown in Fig. 2.

The y-axis of Fig. 2 starts at zero eccentricity corresponding to a circular HPE covariance ellipse, and approaches 1 as the HPE covariance ellipse elongates. The x-axis on Fig. 2 captures orientation of the ellipse, where 0°, and 90° correspond to uncorrelated errors, and anything in between 0°, and 90° corresponds to correlated East-North errors.

Figure 2 shows contours of HPL ratios between baseline and generalized chi-square. All HPL ratio contours have values greater than 1, which is consistent with the proof in Fig. 1. The baseline HPL is most conservative when the HPE covariance ellipse is circular ($e = 0$). The baseline HPL bound then becomes tighter as the HPE covariance ellipse elongates ($e \to 1$). HPL ratios are independent of HPE covariance ellipse orientation. Further analytical evaluation can be found in Appendix A.

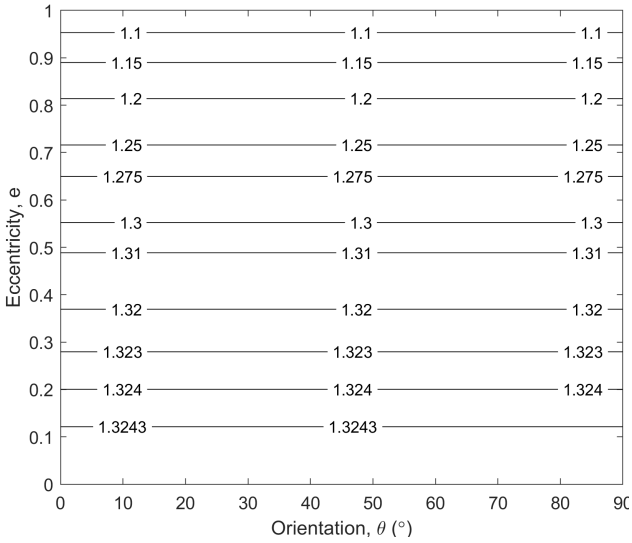

Figure 2: Contours of HPL ratios Eq. (18) for the aleatory HPE covariance ellipse, for a range of eccentricity, and orientation values.

4. Tightness of Baseline HPL for a Realistic Range of Risk Requirements

In this section, we assess the tightness of the baseline HPL with respect to varying risk allocations. Using fixed values for eccentricity, we compute the HPL ratio in Eq. (18) for a set of risk allocations between 10^{-7} and 10^{-3}.

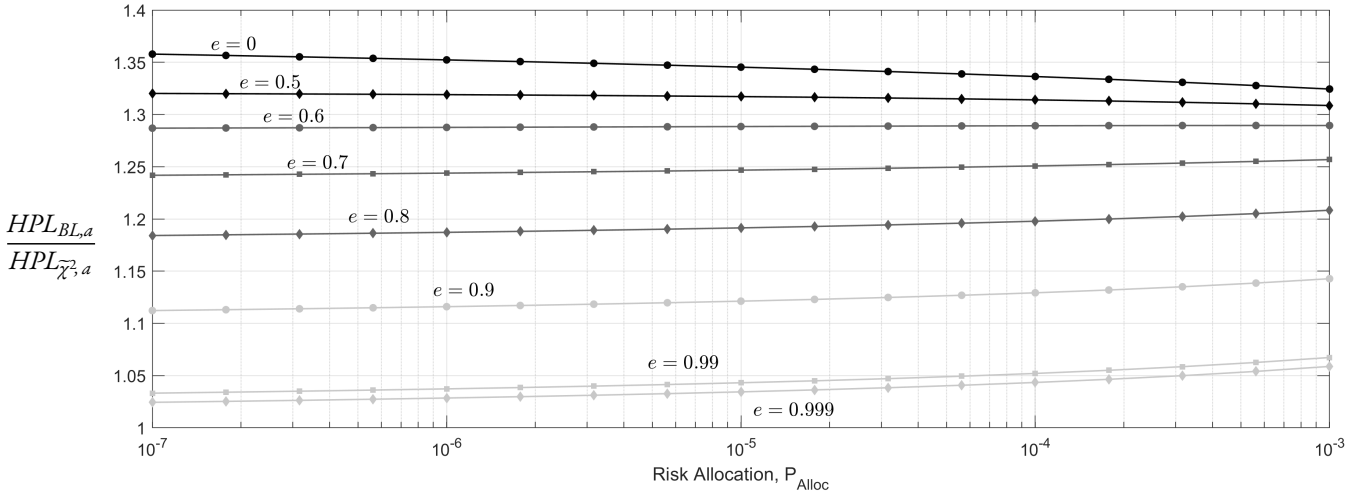

Figure 3: HPL ratios plotted with respect to increasing risk allocation, for different fixed values of eccentricity

Figure 3 shows that the baseline HPL is consistently bounding for the set of risk allocations considered, and that it is most conservative at zero eccentricity (consistent with Fig. 2). At the 10^{-7} risk requirement, we see baseline HPL values that can be around 10% looser for $e = 0.9$, and over 35% looser for $e = 0$.

IV. A TIGHTER AND MORE COMPUTATIONALLY EFFICIENT HPL

1. Baseline Multiple Hypothesis HPL Computation

The baseline ARAIM algorithm iteratively computes a single PL considering all hypotheses $H^{(i)}$, for $i = 1, ..., h$ where h is the number of monitored hypotheses. This is equivalent to optimally allocating the integrity requirement across all h hypotheses for PL evaluation. This process is performed twice, along the East and then North directions, to get the final baseline HPL from Eq. (11). The baseline ARAIM PL equations are

$$\frac{1}{2}P_{Alloc} = \sum_{i=0}^{h} P\left(|\varepsilon_E^{(i)}| \geq PL_E \ \cap \ H^{(i)}\right) \tag{21}$$

$$\frac{1}{2}P_{Alloc} = \sum_{i=0}^{h} P\left(|\varepsilon_N^{(i)}| \geq PL_N \ \cap \ H^{(i)}\right) \tag{22}$$

where the right hand side takes the sum of risks of East/North errors exceeding their associated PL. Combining PLs optimized for East and North directions separately is suboptimal with respect to the radial HPE.

2. New Multiple-Hypothesis HPL Computation

We develop a new approach where the HPL is directly derived from the radial HPE. Another way to express this idea is that the optimal integrity risk allocation across hypotheses is directly performed for the HPE vector magnitude instead of for two separate horizontal directions. Thus, we iteratively solve a single HPL equation instead of two. The new HPL equation is:

$$\frac{1}{2}P_{Alloc} = \sum_{i=0}^{h} P\left(|\varepsilon_{new}^{(i)}| \geq \ HPL_{new} \ \cap \ H^{(i)}\right) \ . \tag{23}$$

The proposed approach models the aleatory and epistemic components of the HPE magnitude ε_{new} as follows:

$$\varepsilon_{new} = \varepsilon_{new,a} + \varepsilon_{new,e} \tag{24}$$

$$\varepsilon_{new,a} \sim N\left(0,\ \left(\sigma_E^2 + \sigma_N^2\right)\right) \tag{25}$$

$$|\varepsilon_{new,e}| \leq \sqrt{d_E^2 + d_N^2}\ . \tag{26}$$

Instead of computing HPL_{BL} using two optimized horizontal PL components, we directly bound the radial HPE parameters $\left(\sigma_E^2 + \sigma_N^2\right)$ and $(\sqrt{d_E^2 + d_N^2})$, and then optimally allocate risk across hypotheses only once to compute an HPL. Proof that HPL_{new} adequately bounds the HPE is in Appendix B. The difference between baseline and new approach is summarized in the figure below.

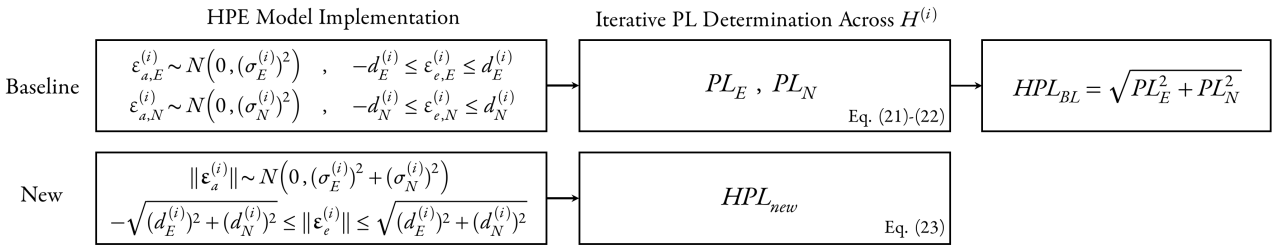

Figure 4: Flowchart comparing baseline HPL approach with proposed new HPL approach

V. HARAIM HPL PERFORMANCE EVALUATION

This section compares HPL_{BL}, HPL_{new}, and $HPL_{\widetilde{\chi}^2}$, and the impacts of HPL_{BL} and HPL_{new} on worldwide ARAIM availability performance. We first consider one location at (50°E, 40°S). We simulate nominal 24-satellite GPS, and 24-satellite Galileo constellations. HPL analysis is performed every minute over 24 hours for HARAIM parameters that can be found in the latest ARAIM ADD (Working Group C (WGC), 2022). Measurement error models follow ED259a (EUROCAE, 2021). Figure 5 is a plot of HPL_{BL}, HPL_{new}, and $HPL_{\widetilde{\chi}^2}$ over twenty four hours. The figure confirms again that both the baseline HPL in gray, and new HPL in black, are always bounding the generalized-chi-square HPL in blue. HPL_{new} actually provides a tighter bound than HPL_{BL}. For sections where HPL_{BL} and HPL_{new} are equal, the new HPL is still more computationally efficient as indicated by the run times in the legend of Fig. 5.

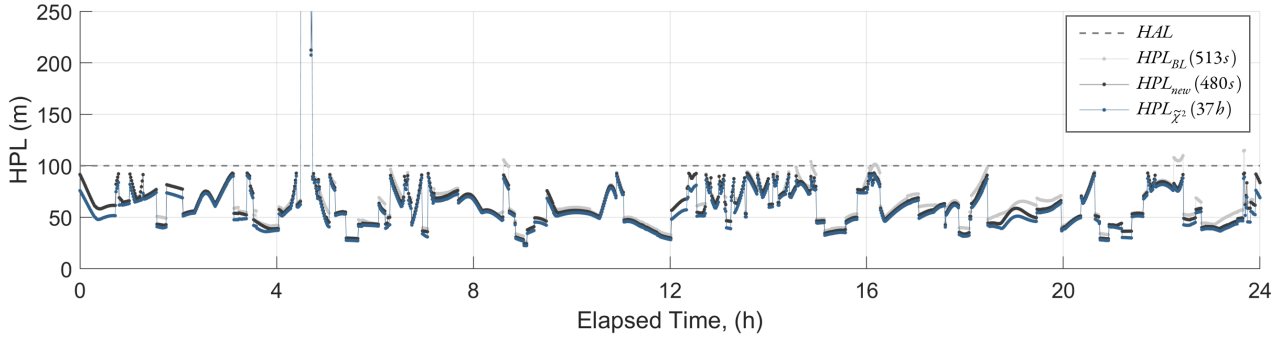

Figure 5: HPL over time at (50°E, 40°S). HPL analysis is performed every minute over 24 hours using 24-GPS, 24-Galileo, ED259a measurement error models, and HARAIM parameters from ARAIM ADD. Simulated using MATLAB 2019a running on Intel(R) Xeon(R) W-2125 CPU @ 4.00GHz, 32.0GB installed RAM, 64-bit operating system, x64-based processor.

We perform HPL analysis for a grid of locations on Earth. Availability is the percentage of time over 24 hours where the computed HPL meets the horizontal alert limit (HAL). In Fig. 6, the color bar indicates a range of availability values from 93% in red to 100% in blue. The overall performance metric is coverage of 100% availability, which measures the fraction of locations that achieves 100% availability. For the example 100-meter HAL used in Fig. 6, coverage increases from 67%

coverage for the baseline HPL, to 85% for the new HPL. HPL_{new}, which we have proven to be bounding HPL_{BL} for a single hypothesis (Appendix B), provides a tighter, more computationally efficient radial HPE bound over multiple hypotheses. Results for other HARAIM HAL's and coverage definitions are given in Table 1, where RNP stands for Required Navigation Performance.

Figure 5 compared HPL performance at (50°E, 40°S), which corresponds to the worst-case location (hottest point) on the left plot of Fig. 6. At this location, the proposed new HPL can improve availability, e.g. after the 8h mark, and just before the 24h mark, where the baseline HPL exceeds the HAL (dashed horizontal line).

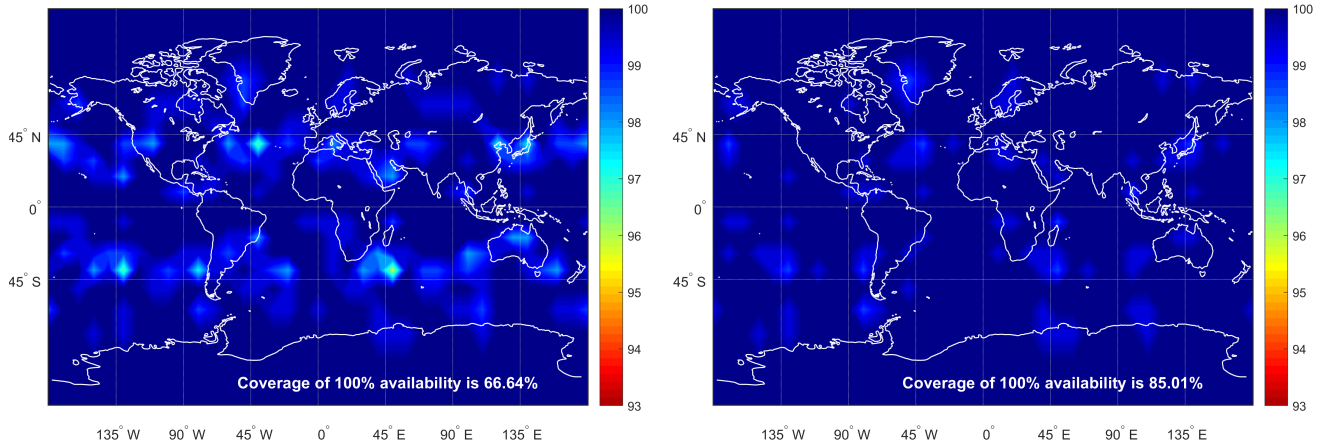

Figure 6: Availability maps of baseline HPL and new HPL for a grid of locations at $10^\circ \times 10^\circ$ latitude-longitude spacing. HPL analysis is performed every 10 minutes over 24 hours using 24-GPS, 24-Galileo, ED259a measurement error models, and HARAIM parameters from ARAIM ADD.

Table 1: Coverage Results for Baseline and New HPL Approaches at Different HARAIM Requirements

	HAL = 100m		RNP 0.1 (185m)		RNP 0.3 (556m)	
	HPL_{BL}	HPL_{new}	HPL_{BL}	HPL_{new}	HPL_{BL}	HPL_{new}
Coverage of 95% Availability	100.00	100.00	100.00	100.00	100.00	100.00
Coverage of 99% Availability	88.8758	98.1997	98.9329	98.9329	99.8138	99.8138
Coverage of 99.5% Availability	66.6447	85.0126	86.3366	86.4197	95.3246	95.3246
Coverage of 100% Availability	66.6447	85.0126	86.3366	86.4197	95.3246	95.3246

VI. CONCLUSIONS

In this paper, we first analyzed the tightness of the baseline HPL as compared to the generalized chi-squared-derived HPL for all HPE covariance ellipse geometries, and for a range of relevant risk allocations. Second, we derived a new HPL equation that requires solving a single iterative HPL equations as opposed to two for the baseline HPL, which is computationally more efficient and can provide a tighter bound. Lastly, we implemented a worldwide availability analysis and showed that the new HPL can improve coverage of 100% availability from 67% using the baseline HPL to as much as 85% for an example 100-meter horizontal alert limit.

APPENDIX A. ANALYTICAL TIGHTNESS EVALUATION FOR LIMIT CASES

1. Limit Case 1: $\lambda_1 = \lambda_2$ ($e = 0$)

Figure 7 illustrates the case where we have a circular HPE covariance ellipse. We compare the generalized chi-square HPL with the baseline HPL. When $\lambda_1 = \lambda_2$, Eq. (16) divided by λ_1^2 becomes a chi-square distribution with two degrees of freedom, χ_2^2. Considering the inverse of the chi-square cumulative distribution function with two degrees of freedom, Eq. (17) has a closed-form solution, and $HPL^2_{\widetilde{\chi}^2,a}$ can be expressed as:

$$\mathrm{cdf}_{\chi_2^2}\left(HPL^2_{\widetilde{\chi}^2,a}/\lambda_1^2\right) = P_{Alloc} \ . \tag{27}$$

In parallel, for $\sigma_E = \sigma_N$, we get $PL_{E,a} = PL_{N,a}$, such that

$$Q\left(\frac{PL_{E,a}}{\sigma_E}\right) = \frac{P_{Alloc}}{4} \ . \tag{28}$$

When $\sigma_E = \sigma_N$, the dashed rectangle in Fig.1 becomes a square, i.e., $HPL_{BL,a} = \sqrt{2}\,PL_{E,a}$. A brief study of bivariate normal distributions shows that for small P_{Alloc}, only a small difference exists between $PL_{E,a}$ and $HPL_{\widetilde{\chi}^2,a}$. This is because the probability density at the intersection of the dashed square and the East or North axis is much higher than near the square's corners. Further contributing to the small difference between $PL_{E,a}$ and $HPL_{\widetilde{\chi}^2,a}$ is the fact that, when building the dashed square, the risk of being in the four dark gray quadrants is double-counted. Therefore, for practical (small) P_{Alloc}, we can write the following approximation:

$$HPL_{BL,a} \approx \sqrt{2}\,HPL_{\widetilde{\chi}^2,a} \ . \tag{29}$$

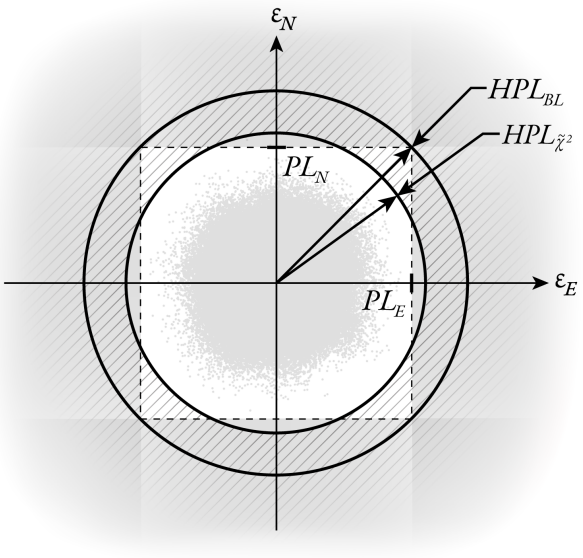

Figure 7: Horizontal positioning error sample distribution given by Eq. (20) for the case where $\lambda_1 = \lambda_2$ ($e = 0$), and any θ

2. Limit Case 2: $\lambda_2 = 0$ ($e \to 1$)

At the limit where $e \to 1$, $\lambda_2 = 0$. Equation (16) simplifies to:

$$\|\boldsymbol{\varepsilon}_a\|^2 = \lambda_1^2 v_1^2 \tag{30}$$

and the HPE distribution approaches a 1D normal distribution given by $\boldsymbol{\varepsilon}_a \sim N\left(0, \lambda_1^2\right)$. Thus, the generalized chi-square HPL becomes:

$$HPL_{\widetilde{\chi}^2,a} = Q^{-1}\left(\frac{P_{Alloc}}{2}\right)\lambda_1 \ . \tag{31}$$

Using the parametrized expression for the alleatory HPE covariance matrix in Eq. (20), the baseline HPL becomes:

$$HPL_{BL,a} = Q^{-1}\left(\frac{P_{Alloc}}{4}\right)\sqrt{\sigma_E^2 + \sigma_N^2} \tag{32}$$

$$= Q^{-1}\left(\frac{P_{Alloc}}{4}\right)\sqrt{\lambda_1^2 \sin^2\theta + \lambda_2^2 \cos^2\theta + \lambda_1^2 \cos^2\theta + \lambda_2^2 \sin^2\theta} \tag{33}$$

$$= Q^{-1}\left(\frac{P_{Alloc}}{4}\right)\lambda_1 \ . \tag{34}$$

Equations (31) and (34) show that, for practical (small) P_{Alloc}, $HPL_{\widetilde{\chi}^2,a} \approx HPL_{BL,a}$.

APPENDIX B. NEW HPL PROOF OF BOUNDING

This appendix shows that for a single hypothesis, the following inequality is always satisfied:

$$HPL_{BL} \leq HPL_{new} \, . \tag{35}$$

HPL_{new} combines bounds on the aleatory and epistemic HPE components in the worst conspiring manner, by taking the sum of their magnitudes, i.e.,

$$HPL_{new} = k\sqrt{\sigma_E^2 + \sigma_N^2} + \sqrt{d_E^2 + d_N^2} \, . \tag{36}$$

Figure 8 graphically shows the following inequality:

$$\sqrt{(k\sigma_E + d_E)^2 + (k\sigma_N + d_N)^2} \leq k\sqrt{\sigma_E^2 + \sigma_N^2} + \sqrt{d_E^2 + d_N^2} \, . \tag{37}$$

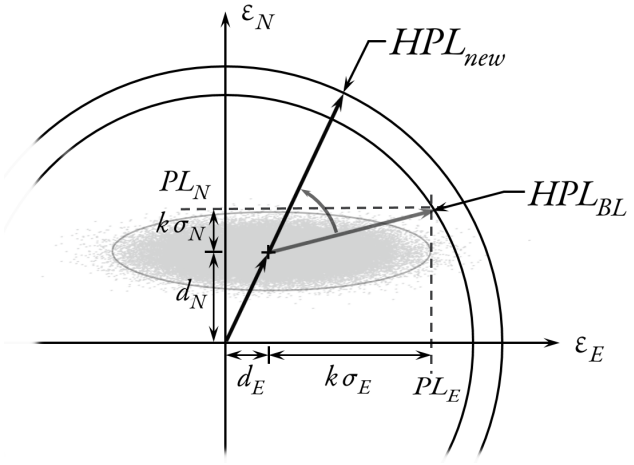

Figure 8: Graphical comparison of HPL_{BL} in gray, and HPL_{new} in black, for an example horizontal positioning error covariance ellipse

ACKNOWLEDGEMENTS

The authors would like to thank the Federal Aviation Administration (FAA) for their support of this research. However, the opinions in this paper are our own and do not necessarily represent those of any other person or organization.

REFERENCES

Blanch, J., Walter, T., Enge, P., Burns, J., Alexander, K., Boyero, J. P., Lee, Y., Pervan, B., Joerger, M., Khanafseh, S., Rippl, M., Martini, I., Perea, S., Kropp, V., Macabiau, C., Suard, N., and Berz, G. (2015). Progress on Working Group-C Activities on Advanced RAIM. In *28th International Technical Meeting of the Satellite Division of the Institute of Navigation (ION GNSS+ 2015)*, pages 629–638, Tampa, Florida.

Davies, R. B. (1980). The Distribution of a Linear Combination of Chi-Square Random Variables. *Journal of the Royal Statistical Society*, 29(3):323–333.

EUROCAE (2021). Minimum Operational Performance Standard for Galileo/Global Positioning System/Satellite-Based Augmentation System Airborne Equipment, ED259a. Technical report.

Jiang, Y. and Wang, J. (2016). A New Approach to Calculate the Horizontal Protection Level. *The Journal of Navigation*, 69:57–74.

Langel, S. (2021). New bounds on the horizontal protection level for the non-zero mean case. In *34th International Technical Meeting of the Satellite Division of the Institute of Navigation, ION GNSS+ 2021*, pages 1565–1576, St. Louis, Missouri.

Ober, P. B. (1997). Ways to improve RAIM/AAIM availability using position domain performance computations. In *1997 National Technical Meeting of The Institute of Navigation*, pages 485–497, Santa Monica, CA.

Radio Technical Commission for Aeronautics (RTCA) Special Committee 159 (2009). Minimum Operational Performance Standards for Global Positioning System/Wide Area Augmentation System Airborne Equipment.

Walter, T. and Enge, P. (1995). Weighted RAIM for Precision Approach. In *8th International Technical Meeting of the Satellite Division of The Institute of Navigation (ION GPS 1995)*, pages 1995–2004, Palm Springs, CA.

Working Group C (WGC) (2016). EU-U.S. Cooperation on Satellite Navigation Working Group C, ARAIM Technical Subgroup, Milestone 3 Report. Technical report.

Working Group C (WGC) (2022). Advanced RAIM Reference Airborne Algorithm Description Document. Technical report.